Wood Science and Technology
https://doi.org/10.1007/s00226-020-01246-6

ORIGINAL

Modelling full-culm bamboo as a naturally varying functionally graded material

Yusuf Akinbade[1] · Ian Nettleship[2] · Christopher Papadopoulos[3] · Kent A. Harries[1]

Received: 14 May 2020 / Accepted: 6 November 2020

Abstract

The mechanical behaviour of bamboo is greatly influenced by its transverse properties, which are not easily measured by experiment. This study develops a framework and the computational tools required to evaluate the material and mechanical properties of bamboo in its full-culm form. A numerical model of bamboo as a transversely isotropic material with functionally graded material properties in the radial direction is developed. The random field method was introduced as a means of quantifying the measured uncertainty of bamboo with respect to the mechanical characterisation of its full-culm state. Four increasingly complex approaches to model circumferential compression tests of bamboo are presented: a theoretical evaluation using Castigliano's theorem; an orthotropic model neglecting the graded nature of the culm wall; and, two models—one discrete and one continuum-based that define a transversely isotropic graded material. Output from each model is compared, calibrated and validated with experimental results. While the models developed were robust, their application has drawn into question the fundamental hypothesis that the functionally graded behaviour of bamboo can be captured using the rule of mixtures.

Introduction

Full-culm bamboo—that is, bamboo used in its natural, round form rather than being processed into an engineered material—used as a structural load-bearing material is receiving considerable attention but has not been widely investigated in a systematic

Electronic supplementary material The online version of this article (https://doi.org/10.1007/s00226-020-01246-6) contains supplementary material, which is available to authorised users.

✉ Kent A. Harries
kharries@pitt.edu

[1] Civil and Environmental Engineering, University of Pittsburgh, Pittsburgh, USA

[2] Mechanical Engineering and Materials Science, University of Pittsburgh, Pittsburgh, USA

[3] University of Puerto Rico at Mayaguez, Mayaguez, Puerto Rico

Published online: 25 November 2020

manner. Van Der Lugt et al. (2003) suggested that bamboo, as a fast-growing renewable material with a simple production process, is a sustainable alternative to more traditional materials like concrete, steel and timber. Despite its availability, sustainability and, in some cases, superior mechanical properties, bamboo is rarely considered by engineers as a building material. This is largely due to the significant gap in data availability and understanding of the material properties and behaviour of bamboo; this gap serves as a primary motivation for this study.

The objective of this study is to illustrate a framework and develop the computational tools required to evaluate the material and mechanical properties of bamboo in its full-culm form. The ability to model and extrapolate standard materials tests with relatively fine-grain modelling, as conducted here, will permit a better understanding of these tests and the application of their derived characteristic properties to the design and macro-scale modelling of bamboo structures. This study reports a numerical model of bamboo as a transversely isotropic material with functionally graded material properties in the radial direction.

Bamboo morphology and microstructure

Bamboo is a functionally graded hierarchical bio-composite (Amada et al. 1996; Ghavami et al. 2003) comprising three fundamental tissues: epidermis, vascular bundles and parenchyma ground tissue. The epidermis is a silica-rich layer comprising the outer wall of the bamboo, which provides environmental protection to the plant. The vascular bundles are the longitudinal tissues supporting the culm, and the ground parenchyma occupies the rest of the culm section (Habibi and Lu 2014). The majority of a bamboo culm section is a composite of vascular bundles embedded in a matrix of parenchyma cells (Liese 1998).

The vascular bundles are composed of metaxylem vessels and sheaths of sclerenchyma fibres. The sclerenchyma fibres are the main longitudinal load-carrying component determining the mechanical characteristics of bamboo, and the parenchyma tissue takes the role of the composite matrix: providing stability to the fibres and transmitting load between them. In the vascular bundle, the vessels transport nutrients and water in the live plant are voids in the material cross section. The macro-mechanical behaviour of bamboo is most often described as a unidirectional fibre reinforced composite material. Its mechanical properties depend on the mechanical characteristics of its components, as well as on its microstructural characteristics, such as the volume fraction and distribution of sclerenchyma fibres, and the interface properties of the various bamboo components (Shao et al. 2010).

Despite prior study of the effect of fibre volume fraction and gradation on the strength of bamboo, results are variable, not well understood, and in some cases contradictory (Akinbade et al. 2019). Additionally, most work has been conducted on a limited number of bamboo species, requiring extrapolation and judgement to extend results to other species or even to the same species harvested in a different location. The objective of this study is therefore to develop a framework and the computational tools required to evaluate the material and mechanical properties of bamboo in its full-culm form. This framework brings together work conducted in the

area of bamboo characterisation (Akinbade et al. 2019, 2020; Gauss et al. 2019) to develop a correlation with the mechanical properties.

Numeric modelling of bamboo

Bamboo is a transversely anisotropic material with differing properties in the longitudinal, radial and circumferential directions. Together, radial and circumferential properties are often referred to as transverse properties. This is partially because a number of experimental studies using small specimens to assess these properties have not adequately differentiated between the radial and circumferential orientations. Due to their dominance, properties in the longitudinal direction have typically been the focus of research studies (an extensive review is provided in Akinbade 2020) and material test methods (ISO 2019). Nonetheless, transverse properties are known to be equally (or perhaps more) important to structural behaviour but more difficult to obtain. Occasionally, the finite element method (FEM) has been adopted to assess transverse mechanical properties although such studies are limited.

Much work in the area of modelling natural materials and natural fibres tends to focus on simplified analytical models; that is, using macro-elements that capture the bulk behaviour of the material (Amada et al. 1996). This approach is likely appropriate when considering engineering structures but may be inadequate when considering materials test methods—from which material properties are obtained—which use small specimens and are influenced by multiple local effects (Richard and Harries 2015; Moran et al. 2017).

Torres et al. (2007) and García et al. (2012) employed transversely isotropic models to simulate bamboo. In this modelling approach, the transverse plane perpendicular to the longitudinal axis of the culm is considered to be isotropic and the mechanical properties in the radial direction are assumed equal to those in the circumferential direction. This approach neglects the functionally graded nature of bamboo in the radial direction.

Santare and Lambros (2000) and Kim and Paulino (2002) developed formulations which automatically interpolate mechanical properties within a graded element. Santare and Lambros sampled the mechanical properties directly at the integration points of the element, while Kim and Paulino adopted a generalised isoparametric formulation. Both found that the solution quality was improved based on the same mesh density, especially for higher-order graded elements. Assigning spatially varying properties at integration points by defining properties as a function of temperature was demonstrated by Rousseau and Tippur (2000). This technique, however, is unable to define a nonlinear continuous variation of the elastic properties in most FEM codes and does not allow for differences in the gradient profile of different properties: Young's modulus and Poisson's ratio, for instance.

Silva et al. (2006) used graded finite elements to capture the varying material property distribution through the bamboo culm wall, comparing results from a spatially varying Young's modulus, an averaged Young's modulus, and orthotropic constitutive properties obtained from homogenisation. It was found that other than the homogenisation technique, which requires additional computational effort, the

elastic modulus resulting from the other methods provided suitable numerical accuracy for capturing the "global" deflection response of a bamboo structure. In addition, Silva et al. (2006) concluded that to accurately estimate local features in the material it is necessary to employ a numerical procedure that accurately models material gradients through the culm wall.

Martínez-Pañeda and Gallego (2015) reviewed different methods by which functionally graded materials have being modelled and concluded that the UMAT and the USDFLD user subroutines in the ABAQUS (2017) software were most versatile. Due to the availability and versatility of the ABAQUS software, it was selected to conduct the numerical analysis presented in this study.

Uncertainty in bamboo materials characterisation

As a functionally graded material, bamboo evolves according to the need to resist external loads and internal stresses resulting from its natural environment (Amada and Untao 2001). Nogata and Takahashi (1995), for instance, showed a variation in vascular bundle arrangement and shape of bamboo grown on steep ground. Other studies have considered the effects of intentionally shaping bamboo culms (Ghavami et al. 2003; Vittouris and Richardson 2011) and the section morphology of [naturally occurring] "square bamboo" (Shigematsu 1958). These studies show marked differences in fibre bundle distribution around the perimeter of the artificial or natural polygonal shaped bamboo, especially at corners. This suggests the importance of growth conditions on the volume fraction of fibres and their distribution from the mechanical and morphological points of view.

Prior research has shown that age at harvesting is also an important factor when considering the strength of bamboo. Sekhar and Bhartari (1960) noted that strength of bamboo increases with age as the plant lignifies, peaking at 2.5–4 years (likely species and growth condition dependent) and then decreases following maturity (reported to be greater than about 6 years). Low et al. (2006) reported a contrary trend, in which modulus of elasticity, strength, and fracture toughness of *N. affinis* were all greater in a one-year-old sample as compared to a matured, five-year-old sample. Correal and Arbelaez (2010) found no correlation between age and modulus of elasticity in bending or compression of *G. angustifolia*. Additionally, bamboo strength and modulus is known to increase with height along the culm (Liese 1998; Sattar et al. 1990; Correal and Arbelaez 2010; Harries et al. 2017).

Similar to wood, moisture content (MC), in addition to the combination of MC and ambient temperature (Gonzalez et al. 2018), affects the properties of bamboo. Conventionally normalised at MC = 12%, mechanical properties of bamboo degrade significantly with increased MC up to about MC = 30%, a value close to the fibre saturation point (FSP) (Janssen 1981; Xu et al. 2014). Like timber, for MC greater than the FSP, further degradation of mechanical properties, while apparent, is less significant.

This all serves to highlight the variability of bamboo and the uncertainty associated with attributing general behaviours or trends to bamboo as a whole. No known studies have addressed uncertainty associated with modelling bamboo. This study will attempt to address this shortcoming using a random fields approach (Alder and Taylor 2010), which has been successfully applied to a number of engineering problems which exhibit high variability and spatial gradation, including pavement (Caro et al. 2014), soils (Kim 2005) and ground water modelling (El-Kadi and Williams 2000).

Calibration test data

Material properties

ISO 22157 standard circumferential compression tests (ISO 2019) of samples of *P. nigra* were conducted to serve as validation cases for this study. This test applies diametric compression across a short ($H = 0.2D$) full-culm specimen (Fig. 1a). Quadrants are designated N–S–E–W, and the load is applied across the N–S diameter. The failure mechanism involves the formation of a pair of multi-pinned arches resulting from hinges forming at the locations of maximum moment around the circumference—the N–S–E–W quadrants—of the culm section. From this, the culm wall bending properties are determined. Specifically, the culm wall modulus of rupture is a measure of the transverse tension capacity of the culm wall and therefore should be correlated with the splitting behaviour. Values of interest from the test are the apparent bending strength perpendicular to the fibres, $f_{m,90}$, and the corresponding circumferential modulus of elasticity, $E_{m,90}$. Calculation of these values from test parameters is given in Online Resource 1. Sharma et al. (2013) and Moran et al. (2017) provide detailed descriptions of this test method and the derivation of properties determined from it. Tests were conducted in a 45 kN-capacity precision gear-driven test frame using a load cell

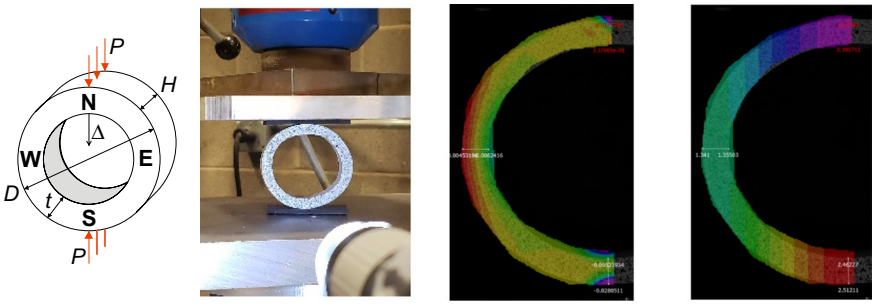

(a) Test set-up showing speckle patten used for DIC

(b) vertical strain field range shown: 0.0043 (red) to -0.0172 (purple)

(c) vertical displacement range shown: 2.47 mm (red) to 0.38 mm (purple)

Fig. 1 Circumferential compression test

having 0.4 N precision. Due to the very small strains involved, tests are run in displacement control at a rate of 0.76 mm/min. Full-field strain measurements of the culm section using a VIC 3D digital image correlation (DIC) system were taken; example strain and vertical displacement images thus obtained are shown in Fig. 1b, c, respectively. A summary of the circumferential compression test results used in this study is given in Table 1; additional details are found in Akinbade (2020). In addition, a larger sample from the same *P. nigra* culms was tested for other material properties also summarised in Table 1 (Akinbade et al. 2019). This latter sample will be collectively referred to as PN in this paper.

Fibre volume fraction

Fibre volume fraction, V_f, of the *P. nigra* samples was determined by image analysis of each quadrant of the specimen as described in Akinbade et al. (2019). For PN, V_f was determined from at least 28 culm wall sections images. The average fibre volume fraction in the section and the best-fit variation through the cross sections are given in Table 2 in which $x = 0$ at the inner culm wall and $x = 1$ at the outer culm wall.

Table 1 Full-culm mechanical properties of *P. nigra* reported in this study (COV provided in parentheses)

Parameter	Units	Sample			
		PN2	PN3	PN4	PN
Density at MC[a] = 12%, ρ_{12}	kg/m^3	907 (0.02)			
MC at test	%	9.1	9.3	8.2	14.8
Diameter[b], D	mm	91.0	90.8	90.5	93.5 (0.03)
Culm wall thickness[c], t	mm	8.35 (0.05)	8.40 (0.01)	8.10 (0.04)	6.74 (0.19)
Ovality[d], d_o		0.09	0.10	0.10	0.08
Specimen length, H	mm	17.2	18.2	19.3	–
Applied load at failure, P	N	383	561	414	–
Deflection at failure, Δ	mm	2.09	3.27	2.07	–
$f_{mC,90,\,EW}$	MPa	− 16.8	− 23.1	− 17.1	–
$f_{mT,90,\,EW}$	MPa	12.2	11.1	12.5	–
$E_{m,90}$	MPa	2623	2351	2658	–
Full-cull compression strength[a], $f_{c,0}$	MPa	–	–	–	45.2 (0.13)
Longitudinal shear[a], f_v	MPa	–	–	–	14.6 (0.16)
Flat ring flexural modulus[a], f_{rC}	MPa	–	–	–	15.6 (0.14)

[a]Data reported in Akinbade et al. (2019)

[b]Average of maximum (D_{max}) and minimum (D_{min}) diameters

[c]Average of four thickness measurements per section

[d]$d_o = 2(D_{max} - D_{min})/(D_{max} + D_{min})$ (ISO 2018)

Table 2 Fibre volume distribution and resulting property distributions through culm wall thickness

Sample	Gross section V_f	$V_f(x)$	$E_T(x)$ (GPa)	$E_L(x)$ (GPa)
PN2	0.28	$1.29x^3 - 1.28x^2 + 0.57x + 0.10$	$21.7x^3 - 23.7x^2 + 7.4x + 1.1$	$43.9x^3 - 43.5x^2 + 19.4x + 4.2$
PN3	0.27	$0.81x^3 - 0.53x^2 + 0.28x + 0.10$	$17.2x^3 - 17.6x^2 + 5.3x + 1.1$	$27.5x^3 - 18.0x^2 + 9.5x + 4.4$
PN4	0.27	$1.09x^3 - 0.90x^2 + 0.40x + 0.10$	$24.1x^3 - 25.9x^2 + 7.7x + 1.1$	$37.1x^3 - 30.6x^2 + 13.6x + 4.5$
PN	0.26	$0.94x^3 - 0.63x^2 + 0.36x + 0.06$	$33.0x^3 - 35.7x^2 + 10.6x + 0.8$	$32.0x^3 - 21.4x^2 + 12.2x + 3.0$
RF1	0.28	$1.29x^3 - 1.28x^2 + 0.57x + 0.10$	$14.6x^3 - 11.8x^2 + 2.6x + 0.4$	$43.9x^3 - 43.5x^2 + 19.4x + 4.2$
RF2			$21.1x^3 - 13.5x^2 + 4.6x + 2.6$	
RF3			$15.4x^3 - 15.3x^2 + 3.9x + 1.7$	
RF4			$8.6x^3 - 3.0x^2 + 0.1x + 1.2$	
RF5			$2.6x^3 + 1.8x^2 - 0.9x + 1.5$	

Modelling the bamboo culm wall

A suite of finite element models of full-culm bamboo was developed and implemented using ABAQUS (2017). In this work, the models have the objective of modelling material test specimen behaviour; specifically, that of the circumferential compression test described in the previous section. The models, which consider non-homogeneous test specimen geometry and capture the functionally graded nature of bamboo, are calibrated using full-field strain data obtained using DIC. The local Cartesian coordinate system, R (radial), C (circumferential) and L (longitudinal), shown in Fig. 2, was adopted using the "material orientation" function in ABAQUS.

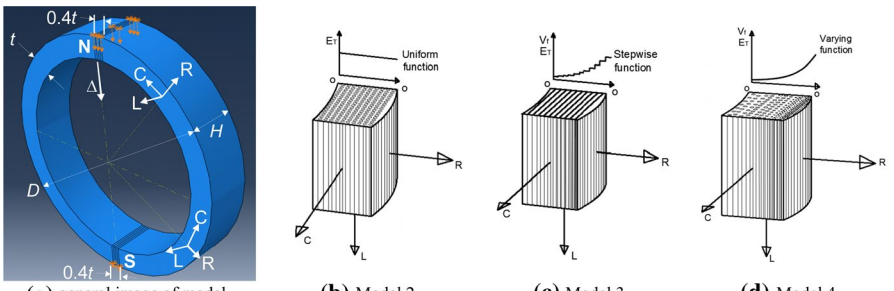

(a) general image of model showing dimensions and local axis orientation **(b)** Model 2 **(c)** Model 3 **(d)** Model 4

Fig. 2 Modelling bamboo as a transversely isotropic material

A naturally isoparametric formulation similar to the one described by Kim and Paulino (2002) is implemented using ABAQUS user-defined subroutine UMAT. UMAT assigns the material parameters directly at the integration points of each element and allows properties to be defined with continuous spatial variation in all directions. The USDFLD subroutine can also be used to accomplish the same modelling objective—yielding essentially identical results—although UMAT was shown to be a simpler implementation (Akinbade 2020) and is reported here.

A linear three-dimensional continuum eight-node brick element (C3D8) is used as a base element. A reduced integration element (C3D8R) was initially considered, but this was found to not fully capture the material strains at the extreme edges of the culm wall. A twenty-node quadratic brick element (C3D20) was also tried exhibiting negligible differences in results from the eight-node element. A hexahedral mesh was chosen due to its better convergence over tetrahedral. Mesh size of approximately $0.1t$ (ten elements through the culm wall thickness) was used. Model restraint was provided by applying a $0.4t$ wide fixed boundary condition at the outer face of the lower part of the ring (S in Fig. 2a). Additional details of the ABAQUS models are reported by Akinbade et al. (2019).

The focus of this study is on capturing material test behaviour prior to failure. No failure criteria are applied; rather, the analysis proceeds by assigning a displacement of 1.5 mm to all nodes within a width of approximately $0.4t$ located at the outer face of the upper part of the culm wall ring (N). This simulates a condition occurring before the ultimate capacity of the modelled tests was reached (Δ in Table 1). Measured dimensions of the specimens (Table 1) were used to create each model.

Constitutive equations

For the remainder of this description, the local Cartesian coordinate system, shown in Fig. 2a, is adopted. Bamboo is a functionally graded material assumed to be transversely isotropic with varying properties in the radial direction and is assumed to be elastic to material failure. In this study, considering the small test specimen dimension, no variation of material properties is applied in the longitudinal or circumferential directions. The elasticity tensor (stiffness matrix) for an orthotropic material requires nine independent material constants which is reduced to five for the transversely isotropic case (Bower 2009): $E_C = E_R = E_T$; $\upsilon_{RC} = \upsilon_{CR} = \upsilon_T$; $\upsilon_{LR} = \upsilon_{LC} = \upsilon_{LT}$; $\upsilon_{RL} = \upsilon_{CL} = \upsilon_{TL}$; and E_L. The Poisson's ratios are not symmetric but satisfy the condition, $\upsilon_{TL}/E_T = \upsilon_{LT}/E_L$. The resulting elasticity tensor (Eq. 1) is in format easily adopted to the material definitions in the ABAQUS UMAT subroutine:

$$\mathbf{K} = \begin{bmatrix} E_T\left(1-\nu_{TL}\nu_{LT}\right)\varphi & E_T\left(\nu_T+\nu_{TL}\nu_{LT}\right)\varphi & E_T\left(\nu_{LT}+\nu_T\nu_{LT}\right)\varphi & 0 & 0 & 0 \\ \cdot & E_T\left(1-\nu_{TL}\nu_{LT}\right)\varphi & E_T\left(\nu_{LT}+\nu_T\nu_{LT}\right)\varphi & 0 & 0 & 0 \\ \cdot & \cdot & E_L\left(1-\nu_T^2\right)\varphi & 0 & 0 & 0 \\ \cdot & \cdot & \cdot & G_{TL} & 0 & 0 \\ \cdot & \text{symmetric} & \cdot & \cdot & G_{TL} & 0 \\ \cdot & \cdot & \cdot & \cdot & \cdot & G_T \end{bmatrix} \tag{1}$$

in which $\varphi = (1 - \upsilon_T^2 - 2\upsilon_{TL}\upsilon_{LT} - 2\upsilon_T\upsilon_{TL}\upsilon_{LT})^{-1}$; $G_{TL} = E_L/(2+2\upsilon_{TL})$; and $G_T = E_T/(2+2\upsilon_T)$.

Parametric definition and calibration

The values of moduli $E_T$and E_L are determined from the rule of mixtures using the fibre volume fraction, V_f, and E_m and E_f, the moduli of the parenchyma matrix and sclerenchyma fibres, respectively (Halpin and Kadros 1976):

$$E_T = \frac{E_E\left(1 + \xi n V_f\right)}{\left(1 - nV_f\right)} \tag{2}$$

where

$$n = \frac{(E_f/E_m - 1)}{(E_f/E_m + \xi)} \tag{3}$$

The value of ξ is an empirical constant fitted to the elasticity solution for a fibre geometry and confirmed by experimental data (Halpin and Kadros 1976; Hewitt and de Malherbe 1970):

$$\xi = \begin{cases} 2 & V_f \le 0.5 \\ 2 + 40V_f^{10} & V_f > 0.5 \end{cases} \tag{4}$$

Longitudinal properties are given by the conventional rule of mixtures:

$$E_L = V_f E_f + \left(1 - V_f\right)E_m \tag{5}$$

Reported values of both E_f and E_m vary (Akinbade 2020). The values $E_f = 35$ GPa and $E_m = 1.8$ GPa, recommended by Janssen (2000), are commonly accepted. Janssen derived these based on longitudinal material properties of bamboo, which are dominated by the value of E_f and modelled well using Eq. 5. On the other hand, the transverse behaviour considered in this study is very sensitive to the value of E_m. Using Janssen's values, an initial modelling campaign indicated predicted behaviour that was stiffer than that experimentally observed by a factor of about 1.7. A calibration was undertaken in which $E_f = 35$ GPa and E_m were calibrated such that the stiffness of the models better matches the experimental data. A value of $E_m = 1.0$ GPa was found to be appropriate for the *P. nigra* material considered and was adopted; this value remains in the range of reported values from the literature (Akinbade 2020).

FE models

FE model complexity is considered using three modelling scenarios in addition to a theoretical approach, all described as follows:

Model 1

Model 1 is a theoretical evaluation in which Castigliano's second theorem (Young et al. 2002) for a thin-walled ring subject to diametrically oriented compression was applied to the circumferential compression test specimens modelled. The equations, presented in Online Resource 1, assume homogenous transverse material properties. Model 1 is presented since this is the same approach used to process test data. Model 1 is also a hand-calculation validation of Model 2, which should yield similar results.

Model 2

Model 2 is an FE model in which cross section orthotropic mechanical properties are calculated using the gross section fibre volume fraction (Table 2) and Eqs. 2 and 5. Resulting constitutive properties (Eq. 1) are given in Online Resource 2 for the four test specimens described in Table 1. Model 2 is an improvement on a homogeneous material as it takes into account the expected material property variation of bamboo in different directions but does not capture the graded nature of the culm wall. Model 2 is illustrated schematically in Fig. 2b.

Model 3

Model 3 is an FE model in which the culm wall is divided into ten concentric annular rings and assigns these average orthotropic mechanical properties based on rule of mixtures refined for volume fractions determined for each concentric section. This results in distribution of properties through the culm wall thickness represented by ten discrete steps as illustrated schematically in Fig. 2c. Constitutive properties (Eq. 1) are given in Online Resource 2 for the four test specimens described in Table 1.

Model 4

Model 4 is an FE model, which implements user-defined mechanical properties (UMAT) through the culm wall thickness, assigning material parameters directly at the integration points of the elements. The cubic representations of E_L and E_T, given in Table 2, are used and, from these, the assumed constitutive equations for a transversely isotropic material (Eq. 1) are calculated. The approach assigns and updates the stress and strain vectors, and other solution-dependent variables over the element volume at the integration points (ABAQUS 2017). The ABAQUS UMAT subroutine is used to program a 3D brick graded finite element having a smooth variation of elastic properties (Fig. 2d). The UMAT subroutine script is given by Akinbade (2020).

Modelling the circumferential compression tests

To validate the modelling approaches, three individual *P. nigra* test specimens (PN2, PN3 and PN4) and a prototype specimen (PN) based on consolidated data from a group of specimens are modelled as summarised in Tables 1 and 2. A summary of the FE-predicted and experimentally obtained results is given in Table 3. The model was simulated for the deflection $\Delta = 1.5$ mm, which is about 70% of the maximum displacement reported (Table 1). DIC-obtained strain data are available for all specimens except PN.

Similar and expected behaviour was observed in all models with the location of the maximum tensile strain at the inner surfaces of the N and S quadrants, while the maximum compressive strain occurred at inner surfaces of the E and W quadrants. At the E (or W, the models are symmetric) quadrant, the maximum compressive strain ranged from − 5000 $\mu\varepsilon$ in Model 2 and increased in Models 3 and 4, having similar values of approximately − 6100 $\mu\varepsilon$. These values all exceeded the DIC-measured values of about − 4500 $\mu\varepsilon$. The maximum tensile strain at the *E* quadrant ranged from about 3700 $\mu\varepsilon$ in Model 2 and decreased to similar values of approximately 2700 $\mu\varepsilon$ in Models 3 and 4—very close to the values measured using DIC, which averaged about 2800 $\mu\varepsilon$. As shown in Table 3, the greater compressive strain and similar tensile strain result in a greater predicted shift in the neutral axis towards the outer culm wall. Model 2 predicts a neutral axis location of 0.52*t*, Models 3 and 4 predict 0.64*t*, while the experimentally observed behaviour ranges from 0.50*t* to 0.56*t*.

A range of maximum compressive stress at the *E* quadrant (inner culm wall surface; $x = 0$) is observed with a value of − 12.4 MPa in Model 2 falling to approximately − 8.5 MPa in Model 3 and − 7.0 MPa in Model 4. Similarly, the maximum tensile stress (outer culm wall surface; $x = 1$) was 9.1 MPa in Model 2, increasing to 14.4 MPa in Model 3 and 17 MPa in Model 4. The models were calibrated such that the average circumferential moduli of the model and that obtained from the experiment were essentially the same. Despite the differences in strains and stresses, the average circumferential modulus, $E_{m,90}$ determined from the experiment (Eq. 2) is similar to that determined from the models with an error ranging from approximately 2% in Model 1 to 4% in Models 3 and 4, and 6% in Model 2.

The circumferential strain distributions at the E quadrant of all models are shown in Fig. 3. In terms of strain distribution, Model 2 has lower values than the experimental data at the inner culm wall and higher values at the outer wall although with only a slight shift in the resulting neutral axis location. Essentially Model 2 predicts similar behaviour to the experiment but with a 'steeper' strain gradient. In the present experimental study and those reported in the literature (Sharma et al. 2013; Moran et al. 2017), the circumferential strain profiles were generally found to shift towards the outer wall. This behaviour was captured in the FE models. Models 3 and 4 behave similarly with essentially identical values although all strains are shifted towards compression and, as a result, the neutral axis location is shifted further towards the outer culm wall. All FE models predict

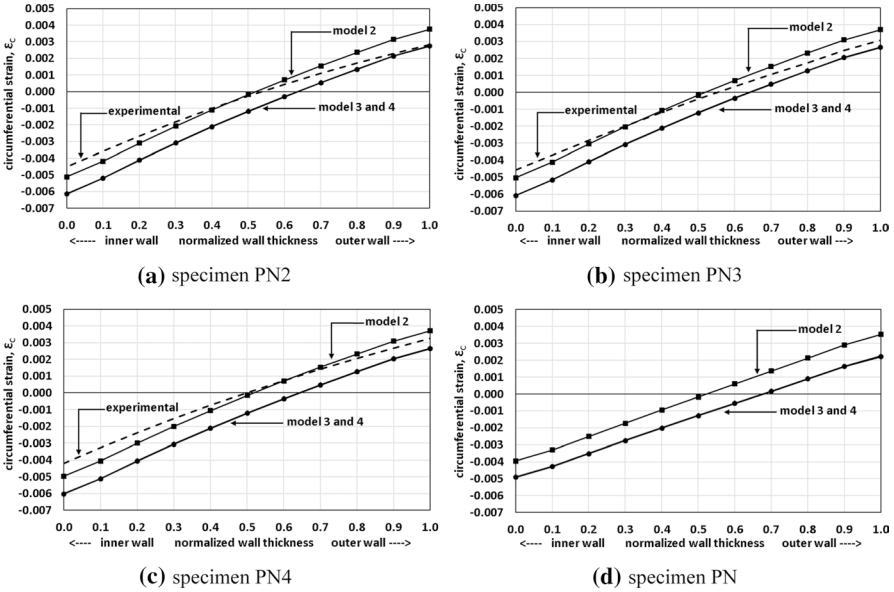

Fig. 3 Circumferential strain distribution at the E quadrant

a 'steeper' strain gradient than the experimental data. Such behaviour suggests the FE model is 'softer' in transverse compression and 'stiffer' in transverse tension than the experimental data reveal. This observation would appear to support modelling bamboo using a bimodular approach: assigning different modulus for tension and compression response as very recently proposed by Lorenzo et al. (2020). Nonetheless, the behaviour shown in Fig. 3 is promising and shows a relatively good comparison with experimental data after only limited calibration. The greatest difference between experimental results and the FE models was about 1500 $\mu\varepsilon$.

Inherent simplification

There are a number of simplifications inherent in the FE models, which are likely to contribute to the efficacy of the specimen-specific models used in this validation. The specimen FE models are simplified as round hollow cylinders having constant wall thickness. The experimental specimens exhibit some degree of ovality (ISO 2018) and variation in wall thickness as given in Table 1. Both will result in variation from the ideal FE culm. Similarly, the distribution of fibre volume fraction is assumed to be uniform around the entire culm circumference.

Nonetheless, the output from the simulations are relatively close to the values reported from the experiments. Model 2 results—which considers the bamboo as

Table 3 Stresses and strains from the E quadrant of the specimens at a prescribed displacement $\Delta = 1.5$ mm

	Sample	Experimental[a]	Model 1	Model 2	Model 3	Model 4
Applied load to cause $\Delta = 1.5$ mm, N	PN2	293.7	288.5	310.8	305.7	306.0
	PN3	300.0	294.3	307.2	296.7	297.2
	PN4	315.0	303.4	326.3	321.5	321.9
	PN	–	152.9	184.5	169.1	168.9
Circumferentially oriented compressive strain at E quadrant, ε_c, $\mu\varepsilon$	PN2	− 4498	–	− 5108	− 6115	− 6144
	PN3	− 4562	–	− 5029	− 6060	− 6084
	PN4	− 4185	–	− 4957	− 6002	− 6031
	PN	–	–	− 3957	− 4894	− 4922
Circumferentially oriented tensile strain at E quadrant, ε_c, $\mu\varepsilon$	PN2	2832	–	3757	2768	2741
	PN3	3064	–	3692	2672	2650
	PN4	3256	–	3698	2660	2633
	PN	–	–	3529	2239	2209
Neutral axis location, x	PN2	0.54t	0.52t	0.52t	0.65t	0.65t
	PN3	0.56t	0.52t	0.52t	0.64t	0.64t
	PN4	0.50t	0.52t	0.52t	0.65t	0.65t
	PN	–	0.52t	0.52t	0.67t	0.67t
Compressive stress at E quadrant, $f_{mC,90,EW}$, MPa (Eq. A.5a)	PN2	− 12.9	− 12.7	− 12.4	− 8.5	− 6.9
	PN3	− 12.1	− 12.1	− 11.5	− 7.9	− 6.8
	PN4	− 12.9	− 12.5	− 12.3	− 8.4	− 6.8
	PN	–	− 9.7	− 10.5	− 6.0	− 4.1
Tensile stress at E quadrant, $f_{mT,90,EW}$, MPa (Eq. A.5b)	PN2	9.4	9.2	9.1	14.4	17.1
	PN3	8.9	8.7	8.4	13.0	15.3
	PN4	9.5	9.2	9.1	14.8	17.7
	PN	–	7.6	9.3	15.1	18.3

Table 3 (continued)

	Sample	Experimental[a]	Model 1	Model 2	Model 3	Model 4
Circumferential modulus, $E_{m,90}$, MPa (Eq. A.1)	PN2	2623	2578	2777	2731	2734
	PN3	2354	2432	2539	2452	2456
	PN4	2658	2614	2811	2770	2773
	PN	–	2700	3257	2986	2982

[a]Details reported in Akinbade (2020)

a homogeneous transversely isotropic material—correlate well with Model 1 calculations based on Castigliano's theorem which serves as the basis for Eq. A.1 (Online Resource 1) in which $E_{m,90}$ is equivalent to E_T. Similarly, Models 3 and 4, which considered the effect of the fibre gradation through the culm wall yielded similar results. However, the graded models appear to result in a shift towards compression strains and, as a result, a more pronounced shift in the neutral axis towards the outer culm wall than was observed in the experiments.

It is also important to note the effect of specimen dimension and distribution of the fibre volume fraction through the culm wall. The variations of circumferential stress and strain through the culm wall thickness obtained from Model 4 are shown in Fig. 4. Since specimens from the same full culm were used for PN2, PN3 and PN4, it is expected that the fibre volume fraction, although slightly different in each specimen, would be sufficiently similar to have essentially the same behaviour under testing. This was confirmed in the experimental tests conducted (Table 1) and is illustrated in Fig. 4. PN, however, is a prototype obtained from the average geometry and fibre distributions of multiple *P. nigra* specimens (Table 1). The behaviour of PN differs only marginally from the specimen-specific data: the 'slope' of the circumferential strain profile is shallower (Fig. 4a). A notable difference between the three modelled test specimens and the prototypical PN model is that PN has a notable thinner wall. The wall thickness ratio, D/t of the three PN2-4 specimens is approximately 10.9, whereas that for PN is 13.9. Both are 'thin-walled'—typically defined for tubes as $D/t > 10$ and proposed for bamboo as $D/t > 8$ (Harries et al. 2017). However, a greater D/t ratio will lead to the stress distribution at the E or W quadrant being proportionally more dominated by the culm wall flexural response than the compression stress also passing through the section at this location—these are the first and second terms, respectively, of Eq. A.5 (Online Resource 1). Figure 4b shows a similarity in the stress profiles of the PN2-4 specimens with the prototypical PN specimen varying slightly in the compressive region near the inner wall face. Using the PN specimen without experimental verification has shown that the procedure reported in this study can be used to predict full-culm bamboo test specimen behaviour with reasonable reliability.

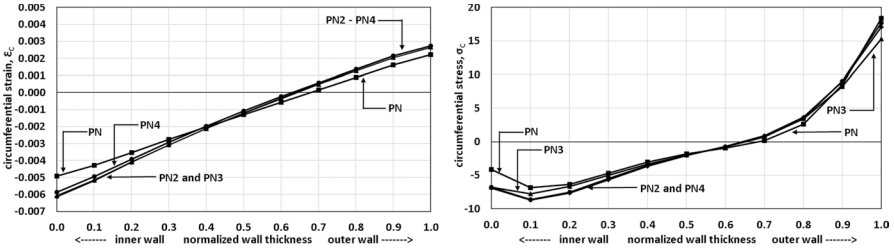

Fig. 4 Circumferential behaviour at the E quadrant predicted using Model 4

Sensitivity analysis of parameters

The reasonable predictive capacity of the closed form solutions of Model 1 permits a rapid assessment of the sensitivity of results to various input parameters. Using the PN model, the following geometric and material properties were each varied ± 20% (a typical coefficient of variation observed for bamboo material properties) to investigate model sensitivity: diameter D, culm wall thickness t, specimen length H, shear modulus G_T, transverse modulus E_T, and longitudinal modulus E_L. This sensitivity analysis was carried out using the equations of Model 1 except for E_L where Model 2 was used. The results are shown in Fig. 5 as normalised values representing the stiffness at a displacement of 1.5 mm plotted against the variation of each parameter.

Specimen stiffness is most sensitive to a change in culm wall thickness, t, varying essentially in proportion to t^3 (that is, in proportion the moment of inertia of the wall section t x H). Specimen stiffness increases 80% with a 20% increase in wall thickness and decreases 50% as the thickness decreases by 20%. Similarly, specimen stiffness varies in an approximately inverse proportional relationship to $1/D^3$. This results in a 44% decrease in stiffness as the diameter increases by 20% and a 105% increase in stiffness as the diameter is reduced by 20%. Both E_T and H exhibit linearly proportional impacts on culm stiffness. The effect of E_L was minimal with a maximum of 2% change in stiffness for a 20% increase or decrease in E_L. G_T had no effect on the stiffness of the specimen over the 20% variation considered. The behaviour again illustrates the importance of wall slenderness, D/t, to culm behaviour. All other parameters being equal, a constant value of D/t results in the same stiffness. It is noted that fundamental behaviour is expected to change as the culm dimensions transition from thin- to thick-walled at around $D/t = 8$ to 10.

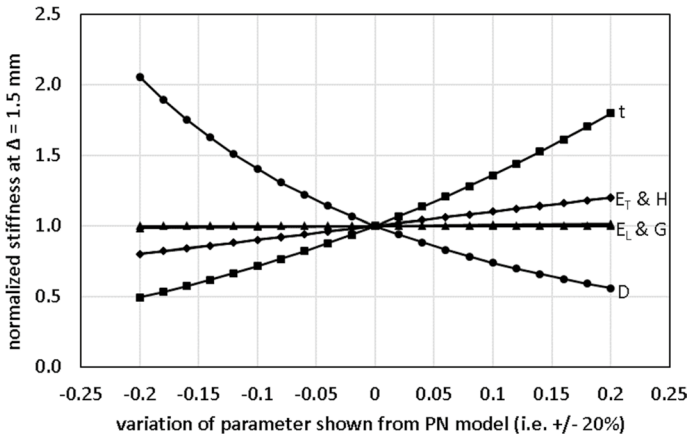

Fig. 5 Sensitivity of circumferential compression test stiffness to bamboo material properties

Random field variables

As the objective of the present modelling approach is to facilitate the ability to model materials test results and extrapolate these, the inherent uncertainty associated with bamboo properties must also be captured. In this study, E_T, which is hypothesised to be a function of the fibre volume fraction, V_f, and therefore varies radially through the bamboo culm wall, is selected. For the random fields approach, the mean value, covariance and spatial dependency (i.e. correlation length of the random field) of E_T, determined from empirical formulae and image analysis, are required. The covariance matrix decomposition technique adopted to generate the random field of E_T is defined as:

$$\mathbf{E_{T,rand}} = \mathbf{CN} + \mathbf{E_{T,mean}} \tag{6}$$

where $\mathbf{E_{T,rand}}$ is the vector containing the values of E_T for the discretised space considered; $\mathbf{N}$ is a vector of normally distributed random values between 0 and 1 (i.e., $N[0,1]$); and $\mathbf{E_{T,mean}}$ is the vector of mean experimentally measured E_T for the discretised space. $\mathbf{C}$ is the autocorrelation matrix obtained from the covariance matrix of the random field $\mathbf{A} = \mathbf{CC^T}$. The Cholesky decomposition matrix technique (Agarwal and Mehra 2014) can be applied to obtain $\mathbf{C}$ from $\mathbf{A}$. The technique is used to decompose the matrix $\mathbf{A}$, which must be symmetric and positive-definite, into an upper and lower triangular matrix of which $\mathbf{C}$ is the lower. The covariance matrix, $\mathbf{A}$, contains information of both the standard deviation, σ, and spatial correlation, $\rho_{i,j}$, of E_T and is defined as:

$$A_{ij} = \sigma^2 \rho_{ij} \tag{7}$$

where $\rho_{i,j}$ = autocorrelation function between each couple of spatial points i and j.

Based on the regression function of V_f given in Table 2, the spatial correlation of E_T is also assumed to be adequately characterised by the cubic correlation function, the isotropic form of which is (Abrahamsen 1997):

$$\rho_{ij} = \begin{cases} 1 - 7\left(\frac{d_{ij}^r}{L_r}\right)^2 + \frac{35}{4}\left(\frac{d_{ij}^r}{L_r}\right)^3 - \frac{7}{2}\left(\frac{d_{ij}^r}{L_r}\right)^5 + \frac{3}{4}\left(\frac{d_{ij}^r}{L_r}\right)^7 & L_r \geq d^r \\ 0 & L_r < d^r \end{cases} \tag{8}$$

where $L_r = t$ is the correlation distance in the radial direction, taken as the culm wall thickness (Akinbade 2020), and $d_{ij}^{\ r}$ is the radial component of the distance between points i and j. The correlation function would include different correlation distances for each direction if an anisotropic random field was being generated. This is useful for a material such as bamboo in which property distributions are known to be highly anisotropic. In this study, however, the variation of properties in the longitudinal direction is not considered due to the relatively short length of the material test specimens being modelled (H) and the transverse distribution is assumed to be radially symmetric.

The foregoing technique is based on the assumption that the spatial correlation can be adequately characterised by the selected correlation function and that

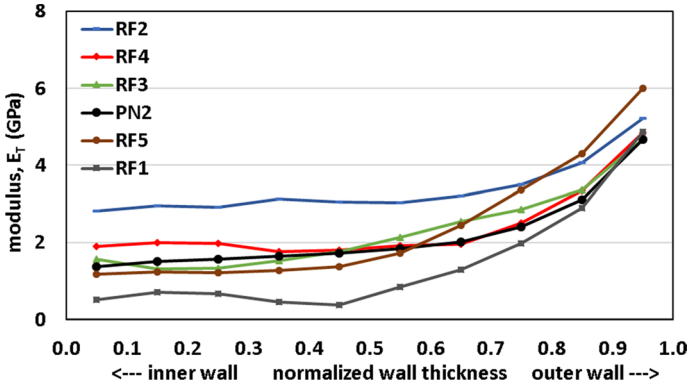

Fig. 6 Random distributions of E_T based on PN2

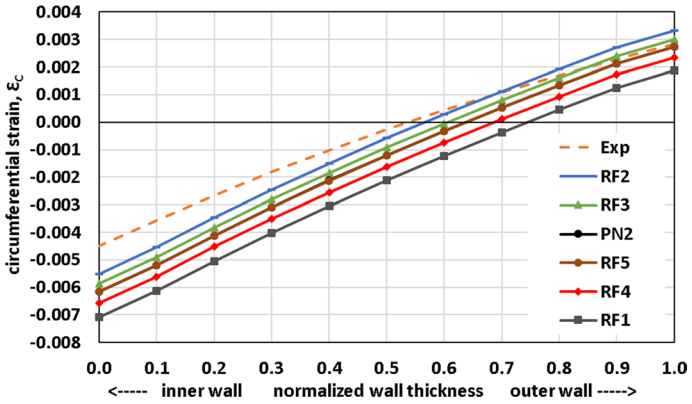

Fig. 7 Circumferential behaviour at the *E* quadrant predicted using Model 4 and randomly generated E_T

the parameter of interest follows a Gaussian distribution. In a recent study which included image analysis of over 3500 culm wall sections, the statistical distribution of both V_f and parameters describing its distribution through the culm wall thickness were confirmed (with 95% confidence) to be Gaussian (Akinbade et al. 2020).

Implementation into FE study

To illustrate the impact of material variability, Models 2 and 4 of sample PN2 were re-run using five random field generated values of E_T. The resulting distributions of E_T, denoted RF1 to RF5, are shown in Fig. 6 and the corresponding cubic functions for E_T are given in Table 2. The results of the analysis are given in Table 4; both the experimental and previously reported PN2 (Table 3) results are repeated for clarity. Circumferential strain distributions resulting from Model 4 are shown in Fig. 7.

Table 4 Stresses and strains from the E quadrant of PN2 for randomly generated E T at a displacement $\Delta = 1.5$ mm

	Exp	Model	PN2	RF1	RF2	RF3	RF4	RF5
Average E_T, MPa	–	–	2473	1634	3469	2534	2579	2417
Applied load to cause $\Delta = 1.5$ mm, N	293.7	2	− 310.8	− 209.3	− 430.2	− 318.2	− 323.6	− 304.0
		4	− 306.0	− 151.2	− 439.1	− 330.6	− 270.7	− 280.9
Circumferentially oriented compressive strain at E quadrant, ε_c, με	–	2	− 5108	− 5156	− 5065	− 5108	− 5106	− 5114
		4	− 6144	− 7081	− 5510	− 5868	− 6569	− 6161
Circumferentially oriented tensile strain at *E* quadrant, ε_c, $\mu\varepsilon$	2832	2	3757	3752	3761	3758	3759	3758
		4	2741	1868	3315	3000	2342	2738
Neutral axis location, x	0.54t	2	0.52t	0.52t	0.52t	0.52t	0.52t	0.52t
		4	0.65t	0.75t	0.57t	0.60t	0.69t	0.65t
Compressive stress at E quadrant, $f_{mC,90,EW}$, MPa (Eq. A.5a)	− 12.9	2	− 12.4	− 8.3	− 17.0	− 12.7	− 13.0	− 12.2
		4	− 6.9	− 3.3	− 14.2	− 10.2	− 7.9	− 9.2
Tensile stress at E quadrant, $f_{mT,90,EW}$, MPa (Eq. A.5b)	9.4	2	9.11	6.00	12.79	9.34	9.50	8.90
		4	17.10	10.35	18.60	16.45	15.5	13.34
Circumferential modulus, $E_{m,90}$, MPa (Eq. A.1)	2623	2	2777	1870	3843	2843	2891	2716
		4	2734	1351	3923	2954	2418	2510

Similar to the results presented previously, changes in stresses, strains and circumferential moduli were exhibited for each randomly generated value of E_T. Each randomly generated polynomial representation of E_T (Fig. 6 and Table 2) is reviewed with its corresponding result to better explain the predicted behaviour; all data are compared to that obtained for PN2.

Because the model deformation is constant ($\Delta = 1.5$ mm) and Model 2 is transversely isotropic, Model 2 strains are not expected to vary from those of PN2, while stresses are proportional to E_T; this is shown in Table 5, which summarises the differences from the PN2 baseline for the five random cases modelled. Model 4, however, captures the effects of varying distribution of E_T.

RF1 exhibits a lower value of E_T at the inner culm wall extending across most of the culm wall and then projects to a marginally higher value towards the outer culm wall (Fig. 6). As a result of the lower average modulus (66% of that of PN2 as shown in Table 5), a lower force is required to achieve $\Delta = 1.5$ mm. Because of the softer response across most of the culm wall, a shift in strains towards compression is observed (Fig. 6) resulting in a significant shift of the neutral axis to $0.75t$. Consistent observations were made for the RF2 case that has relatively higher modulus values across the culm wall (140% of that of PN2). In this case, a stiffer compressive response is predicted resulting in a shift in the strains towards tension and the neutral axis shifting back towards the centre of the wall ($0.57t$).

RF5 is also interesting in that E_T is lower at the inner culm compressive region and higher at the outer culm wall tensile region. This distribution results in a steeper gradient across the culm wall although a similar average modulus to the PN2 baseline case. Despite the deviation in gradient, because the average strain was similar, the predicted strains are close to those of PN2 (Fig. 6). The local stresses are then proportional to the modulus. RF3 and RF4 had very little variation from PN2 in terms of input and model results. Table 5 summarises the ratios of results from the RF cases to those of PN2, all modelled using Model 4. As expected, strains are proportional, and stresses are inversely proportional to modulus. As seen in Table 5, the effect of variation through the culm wall can significantly affect the ratios observed although expected proportionalities are maintained.

Conclusion

The objective of this study was to illustrate a framework and develop the computational tools required to evaluate the material and mechanical properties of bamboo in its full-culm form. The ability to model and extrapolate standard materials tests with relatively fine-grain modelling will permit a better understanding of these tests and the application of their derived characteristic properties to the design and macro-scale modelling of bamboo structures. This study reports a numerical model of bamboo as a transversely isotropic material with functionally graded material properties in the radial direction. The modelling approach demonstrated is intended to provide a tool to expand the understanding of bamboo behaviour by providing a virtual means of augmenting materials test data. Through such an approach, for

Table 5 Ratio of random field results from Models 2 and 4 to those of the baseline PN2 Model

	Model 2					Model 4				
	RF1	RF2	RF3	RF4	RF5	RF1	RF2	RF3	RF4	RF5
Average E_T	0.66	1.40	1.02	1.04	0.98	0.66	1.40	1.02	1.04	0.98
Applied load to cause $\Delta = 1.5$ mm, N	0.67	1.38	1.02	1.04	0.98	0.49	1.43	1.08	0.88	0.92
Circumferentially oriented compressive strain at E quadrant, ε_c, $\mu\varepsilon$	1.01	0.99	1.00	1.00	1.00	1.15	0.90	0.96	1.07	1.00
Circumferentially oriented tensile strain at E quadrant, ε_c, $\mu\varepsilon$	1.00	1.00	1.00	1.00	1.00	0.68	1.21	1.09	0.85	1.00
Neutral axis location, x	No change	No change	No change	No change	No change	$+0.10t$	$-0.07t$	$-0.05t$	$+0.04t$	No change
Compressive stress at E quadrant, $f_{mC,90,EW}$, MPa (Eq. A.5a)	0.67	1.37	1.02	1.05	0.98	0.48	2.05	1.47	1.14	1.33
Tensile stress at E quadrant, $f_{mT,90,EW}$, MPa (Eq. A.5b	0.66	1.40	1.03	1.04	0.98	0.61	1.09	0.96	0.91	0.78
A.1)	0.67	1.38	1.02	1.04	0.98	0.49	1.43	1.08	0.88	0.92

instance, hypotheses of damage propagation and failure criteria for bamboo can be tested across a range of parameters including different bamboo species.

Four increasingly complex approaches to model circumferential compression tests of bamboo were presented. Model 1 is a theoretical evaluation using Castigliano's theorem. Model 2 assigns orthotropic mechanical properties of bamboo in a FE model without capturing the graded nature of the culm wall. Model 3 captures the transverse distribution of properties by assigning average orthotropic mechanical properties to a culm wall divided into ten concentric annular ring sections. Finally, Model 4 uses the ABAQUS UMAT subroutine to define a transversely isotropic graded material with properties assigned at integration points of each element. Output from each model is compared, calibrated and validated with DIC and experimental results.

Despite the complexity of the models, a simple calibration with limited experimental data served to establish a robust model. In this case, transverse elastic modulus—calculated from the rule of mixtures (Eq. 2)—was calibrated from results of three circumferential compression tests of *P. nigra* bamboo. Fibre and matrix moduli were estimated to be $E_f = 35$ GPa and $E_m = 1$ GPa, respectively. Using these values, representative fibre volume fraction (V_f) distribution established from simple image analysis, and average geometry, predicted behaviour of a representative prototype test sample (PN) was predicted. The following observations were made:

1. All models represented experimentally observed bamboo behaviour reasonably well although there was a universally observed shift towards compression strains at the inner regions of the culm wall thickness while tension strains were well predicted. This resulted in the models exhibiting a "steeper" strain gradient and an outward shift in the predicted location of the neutral axis compared to that observed in experiments. This global observation supports the adoption of a bimodulus approach to modelling bamboo as has recently been proposed by Lorenzo et al. (2020).
2. Models 1 and 2, based on average material properties without considering a gradient, captured experimental data better than the more complex FE models. This observation, however, needs to be understood in context. All models were calibrated to average values of E_T. The FE models then distributed the modulus using the rule of mixtures maintaining the calculated average value. The fact that the FE models predicted gross section behaviour relatively well but failed to capture observed local effects calls into question the assumptions involved in distributing the graded material properties using the rule of mixtures based on measured fibre volume fraction.
3. Each of Models 3 and 4 performed equally well. Model 3 is a 'brute force' approach ill suited to a robust modelling campaign although useful in validating the numerically more complex Model 4 which is recommended for adoption for further numerical studies of effects of the functionally graded nature of bamboo culms on standard materials test results.
4. The sensitivity of results to the individual input parameters from the geometry and material properties was considered. It was found that the culm wall thickness impacts specimen stiffness proportionally to t^3 (the moment of inertia of the culm

wall) and the diameter impacts stiffness proportionally to $1/D^3$. Thus, all other parameters being equal, a constant value of D/t results in the same stiffness. E_T and H affected stiffness in a linearly proportional manner while E_L and G had essentially no effect on the predicted test specimen stiffness.

Observations 2 and 4 indicate that simple orthotropic section models (Model 2) are sufficiently robust to capture the macro-scale behaviour of the bamboo culm and indeed could be normalised using the ratio D/t to provide even greater utility in modelling full-culm bamboo elements and structures. A more rigorous understanding of materials test data, damage propagation and failure criteria, however, is believed to require capturing the functionally graded behaviour of bamboo that is made possible using the approach of Model 4.

The random field method was introduced as a means of quantifying the measured uncertainty of bamboo with respect to the mechanical characterisation of its full-culm state. An example of the implementation of the covariance matrix decomposition technique was illustrated with radially oriented elastic modulus E_T as the randomised parameter. The following additional observations were made:

5. A cubic correlation function was found to adequately characterise the spatial correlation function of E_T and a correlation distance equal to the bamboo wall thickness, t, was found to be appropriate.
6. The modelling procedure was repeated to demonstrate the random field methodology and to investigate the effect of uncertainty on bamboo transverse behaviour. As expected, it is observed that strains are proportional, and stresses are inversely proportional to modulus. The effect of variation through the culm wall can significantly affect the prediction of experimental results although the same expected proportionalities are maintained.

The primary conclusion of this study is that the transverse mechanical behaviour of bamboo is greatly influenced by its transverse properties, which are not easily measured by experiment. The random field technique applying the rule of mixtures was proposed to address this deficiency. While the models developed were robust, their application has drawn into question the fundamental hypothesis that the functionally graded behaviour of bamboo can be captured using the rule of mixtures. The modelling approach presented provides a vehicle to explore this hypothesis.

Acknowledgements The authors acknowledge the support of the United States National Science Foundation (award number CMMI 1634739).

Compliance with ethical standards

Conflict of interest On behalf of all authors, the corresponding author states that there is no conflict of interest.

References

ABAQUS (2017) *ABAQUS version 6.12 Computer Software*. Dassault Systems, USA.

Abrahamsen P (1997) A review of gaussian random fields and correlation functions. In: *Technical report 917,* Norwegian Computing Center, Oslo

Agarwal M, Mehra R (2014) Review of matrix decomposition techniques for signal processing applications. Int J Eng Res Appl 4(1):90–93

Akinbade Y (2020) Mechanical and morphological characterization of full-culm Bamboo. In: Ph.D. Dissertation, University of Pittsburgh, p. 202

Akinbade Y, Harries KA, Sharma B, Nettleship I, Ramage M (2020) Variation of through-culm wall morphology in *P. edulis* bamboo strips used in glue-laminated bamboo beams. Constr Build Mater 232:117248

Akinbade Y, Harries KA, Flower C, Nettleship I, Papadopoulos C, Platt SP (2019) Through-Culm wall mechanical behaviour of bamboo. Constr Build Mater 216:485–495

Alder RJ, Taylor JE (2010) Random fields and geometry. Springer, New York

Amada S, Munekata T, Nagase Y, Ichikawa Y, Kirigai A, Yang Z (1996) The mechanical structures of bamboos in viewpoint of functionally gradient and composite materials. J Compos Mater 30(7):800–819

Amada S, Untao S (2001) Fracture properties of bamboo. Compos B 32:451

Bower AF (2009) Applied mechanics of solids. CRC Press, New York

Caro S, Castillo D, Sanchez-Silva M (2014) Methodology for modeling the uncertainty of material properties in asphalt pavements. ASCE J Mater Civ Eng 26(3):440–448

Correal JFD, Arbeláez C (2010) Influence of age and height position on Colombian *Guadua angustifolia* bamboo mechanical properties. Maderas Ciencia y tecnología 12(2):105–113

El-Kadi AI, Williams SA (2000) Generating two-dimensional fields of autocorrelated, normally distributed parameters by the matrix decomposition method. Ground Water 38(4):530–532

García JJ, Rangel C, Ghavami K (2012) Experiments with rings to determine the anisotropic elastic constants of bamboo. Constr Build Mater 31:52–57

Gauss C, Savastano H, Harries KA (2019) Use of ISO 22157 mechanical test methods and the characterisation of Brazilian *P. edulis* bamboo. Constr Build Mater 228:116728

Ghavami K, Rodriques CS, Paciornik S (2003) Bamboo: functionally graded composite material. Asian J Civ Eng (Build Housing) 4(1):1–10

Gonzalez MG, Madden J, Maluk C (2018) Experimental study on compressive and tensile strength of bamboo at elevated temperatures. In: World conference on timber engineering, August 20–23, Seoul

Habibi MK, Lu Y (2014) Crack propagation in Bamboo's hierarchical cellular structure. Nat Sci Rep 4:5598. https://doi.org/10.1038/srep05598

Halpin JC, Kardos JL (1976) The Halpin-Tsai equations: a review. Polym Eng Sci 16(5):344–352

Harries KA, Bumstead J, Richard MJ, Trujillo D (2017) Geometric and material effects on bamboo buckling behaviour. ICE Struct Build 170(4):236–249

Hewitt RL, Malherbe MC (1970) An approximation for the longitudinal shear modulus of continuous fiber composites. Compos Mater 4:280

ISO (2019) ISO 22157:2019: Bamboo structures—Determination of physical and mechanical properties of bamboo culms. International Standards Organization, Geneva, Switzerland

ISO (2018) ISO 19624:2018 Bamboo structures—Grading of bamboo culms – Basic principles and procedures. International Standards Organization, Geneva, Switzerland

Janssen JA (1981) Bamboo in building structures. Doctoral Thesis. Eindhoven University of Technology, Netherlands

Janssen JA (2000) Designing and building with bamboo. International Network for Bamboo and Rattan, Technical Report No. 20

Kim H (2005) Spatial variability of soils: stiffness and strength. Ph.D. Dissertation. Georgia Institute of Technology

Kim JH, Paulino GH (2002) Isoparametric graded finite elements for nonhomogeneous isotropic and orthotropic materials. J Appl Mech 69(513):502–514

Liese W (1998) The anatomy of bamboo culms. International Network for Bamboo and Rattans (INBAR), Beijing, Technical report No, p 18

Lorenzo R, Mimendi L, Li H, Yang D (2020) Bimodulus bending model for bamboo poles. Constr Build Mater 262:120876

Low IM, Che ZY, Latella BA (2006) Mapping the structure, composition and mechanical properties of bamboo. J Mater Res 21:1969–1976
Martínez-Pañeda E, Gallego R (2015) Numerical analysis of quasi-static fracture in functionally graded materials. Int J Mech Mater Des 11(4):405–424
Moran R, Webb K, Harries KA, Garcia JJ (2017) Edge bearing tests to characterize the radial gradation of bamboo. Constr Build Mater 131:574–584
Nogata F, Takahashi H (1995) Intelligent functionally graded material: Bamboo. Eng Compos 5:743
Richard MJ, Harries KA (2015) On inherent bending in tension tests of bamboo. Wood Sci Technol 49(1):99–119
Rousseau CE, Tippur HV (2000) Compositionally graded materials with cracks normal to the elastic gradient. Acta Mater 48:4021–4033
Santare MH, Lambros J (2000) Use of graded finite elements to model the behaviour of nonhomogeneous materials. ASME Trans J Appl Mech 67:819–822
Sattar MA, Kabir MF, Bhattacharjee DK (1990) Effect of age and height position of muli (*Melocanna baccifera*) and borak (*Bambusa balcooa*) bamboos on their physical and mechanical properties. Bangladesh J For Sci 19(1/2):29–37
Sekhar AC, Bhartari RK (1960) Studies on strength of bamboos: a note on its mechanical behavior. Indian Forest 86:296–301
Shao ZP, Fang CH, Huang SX, Tian GL (2010) Tensile properties of Moso bamboo (*Phyllostachys pubescens*) and its components with respect to its fiber-reinforced composite structure. Wood Sci Technol 44:655–666
Sharma B, Harries KA, Ghavami K (2013) Methods of Determining Transverse Mechanical Properties of Full-Culm Bamboo. Constr Build Mater 38:627–637
Shigematsu Y (1958) Analytical investigation of the stem form of the important species of bamboo. Bull Faculty Agric Univ Miyazaki 3:124–135 (**(in Japanese)**)
Silva ECN, Walters MC, Paulino GH (2006) Modeling bamboo as a functionally graded material: lessons for the analysis of affordable materials. J Mater Sci 41(21):6991–7004
Torres LA, Ghavami K, Garcia JJ (2007) A transversely isotropic law for the determination of the circumferential young's modulus of bamboo with diametric compression tests. Latin Am Appl Res 37(4):255–260
Van Der Lugt P, Van den Dobbelsteen AAJF, Abrahams R (2003) Bamboo as a building material alternative for Western Europe? A study of the environmental performance, costs and bottlenecks of the use of bamboo (products) in Western Europe. J Bamboo Rattan 2(3):205–223
Vittouris A, Richardson M (2011) Designing vehicles for natural production: growing a velomobile from bamboo. In: Australasian transport research forum, pp 28–30
Xu Q, Harries K, Li X, Liu Q, Gottron J (2014) Mechanical properties of structural bamboo following immersion in water. Eng Struct 81:230–239
Young WC, Budynas RG, Sadegh AM (2002) Roark's formulas for stress and strain, vol 7. McGraw-Hill, New York